

Mode III effects on interface delamination

Viggo Tvergaard^{a,*}, John W. Hutchinson^b

^a*Department of Mechanical Engineering, Solid Mechanics, Technical University of Denmark, DK-2800 Kgs., Lyngby, Denmark*

^b*Division of Engineering and Applied Sciences, Harvard University, Cambridge, MA 02138, USA*

Received 19 December 2006; received in revised form 24 April 2007; accepted 25 April 2007

Abstract

For crack growth along an interface between dissimilar materials the effect of combined modes I, II and III at the crack-tip is investigated. First, in order to highlight situations where crack growth is affected by a mode III contribution, examples of material configurations are discussed where mode III has an effect. Subsequently, the focus is on crack growth along an interface between an elastic-plastic solid and an elastic substrate. The analyses are carried out for conditions of small-scale yielding, with the fracture process at the interface represented by a cohesive zone model. Due to the mismatch of elastic properties across the interface the corresponding elastic solution has an oscillating stress singularity, and this solution is applied as boundary conditions on the outer edge of the region analyzed. For several combinations of modes I, II and III crack growth resistance curves are calculated numerically in order to determine the steady-state fracture toughness. For given values of K_I and K_{II} the minimum fracture toughness corresponds to $K_{III} = 0$ in most of the range analyzed, but there is a range where the minimum occurs for a nonzero value of K_{III} .

© 2007 Elsevier Ltd. All rights reserved.

Keywords: Plasticity; Crack growth; Mixed-mode fracture; Finite strains; Cohesive zone

1. Introduction

The fact that many interfaces are significantly tougher in the presence of a mode II component of stress intensity is well established. Such behavior is represented by an interface cracking criterion of the form

$$G = \Gamma_C(\psi) \quad \text{with } \psi = \tan^{-1}(K_{II}/K_I), \quad (1)$$

where G is the energy release rate for crack advance in the interface, K_I and K_{II} are the mode I and mode II stress intensity factors (Fig. 1), and $\Gamma_C(\psi)$ is the mode dependent interface toughness. Enhanced mode II toughness is associated with a function $\Gamma_C(\psi)$ which increases with $|\psi|$, and a wide variety of interfaces have been observed whose toughness increases under increasing mode II. The most complete experimental measurements have been for epoxy–glass interfaces by Liechti and Chai (1992) and Banks-Sills et al. (1999) where the toughness for interface intensities approaching mode II is about 10 times that for mode I. The physical origin of a mode II toughness enhancement depends on the interface and the materials it joins.

*Corresponding author.

E-mail address: vit@mek.dtu.dk (V. Tvergaard).

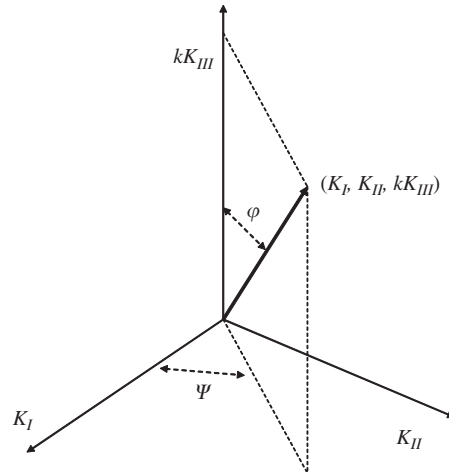


Fig. 1. Conventions for three-mode stress intensities.

For brittle materials, interface roughness can produce mode II interference between crack faces immediately behind the crack-tip, shielding the tip (Evans and Hutchinson, 1989). When either, or both, of the materials joined at the interface experience plastic deformation near the crack-tip, the mode II component produces relatively more plastic dissipation than the mode I component, giving rise to increasing toughness with increasing $|\psi|$ (Tvergaard and Hutchinson, 1993). If the materials are joined by a thin adhesive layer in the interface, the inelastic deformation of the adhesive layer itself can be mode dependent Yang and Thouless (2001).

There is little direct experimental evidence of the role of the mode III component of stress intensity in interface fracture. One exception is the cut test (Jensen et al., 1990) in which a thin film of polyimide bonded to a glass substrate and subject to an equi-biaxial tensile stress is cut along a straight line down to the substrate. If an interface crack spreads from the cut, one possibility is that it arrests in the shape of the delamination shown in Fig. 2. The crack edge experiences all three modes of stress intensity, and Jensen et al. showed that the arrested shape is quite sensitive to the manner in which the interface toughness depends on the mode III component. Mode mixity in thin film debond problems have also been considered by Chai (1990).

As preface to discussing this dependence and in preparation for the general discussion in this paper, the three-mode interface toughness criterion proposed by Jensen et al. (1990) is introduced. At any point along the edge of a three-dimensional interface crack, the energy release rate is

$$G = \frac{1}{2}(1 - \beta^2) \left(\frac{1 - \nu_1^2}{E_1} + \frac{1 - \nu_2^2}{E_2} \right) (K_I^2 + K_{II}^2) + \frac{1}{4} \left(\frac{1}{\mu_1} + \frac{1}{\mu_2} \right) K_{III}^2, \quad (2)$$

where E , μ and ν are Young's modulus, shear modulus and Poisson's ratio of the isotropic solid on the side of the interface as labeled by the subscript. The second Dundurs' parameter, β , is given in the next section. If $\beta = 0$, or if one neglects β^2 compared to 1, the above relation can be written as

$$G = G_I + G_{II} + G_{III} \quad (3)$$

with

$$G_I, G_{II} = \frac{1}{2} \left(\frac{1 - \nu_1^2}{E_1} + \frac{1 - \nu_2^2}{E_2} \right) (K_I^2, K_{II}^2), \quad G_{III} = \frac{1}{4} \left(\frac{1}{\mu_1} + \frac{1}{\mu_2} \right) K_{III}^2. \quad (4)$$

The mixed mode criterion (1) can be generalized to include mode III as

$$G = \Gamma_C(\psi, \varphi), \quad (5)$$

where ψ and φ are the Euler angles in K -space shown in Fig. 1:

$$\psi = \tan^{-1}(K_{II}/K_I),$$

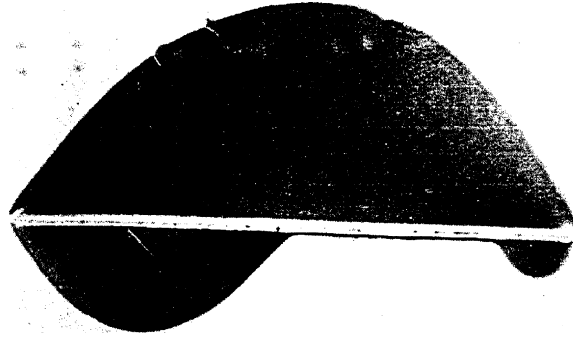


Fig. 2. Delaminations at the interface from a straight cut through a polyimide film bonded to a glass substrate (Jensen et al., 1990).

$$\varphi = \tan^{-1} \left(\sqrt{K_I^2 + K_{II}^2} / kK_{III} \right), (\tan^2 \varphi = (G_I + G_{II}) / G_{III}) \quad (6)$$

with

$$k^2 = \frac{1}{2} \left(\frac{1}{\mu_1} + \frac{1}{\mu_2} \right) \left(\frac{1 - \nu_1^2}{E_1} + \frac{1 - \nu_2^2}{E_2} \right)^{-1}.$$

The phenomenological three-mode interface fracture criterion used more than any other to date because of its mathematical simplicity is

$$G_I + \kappa_{II} G_{II} + \kappa_{III} G_{III} = \Gamma_{IC}, \quad (7)$$

where Γ_{IC} is the mode I toughness and Γ_{IC}/κ_{II} and Γ_{IC}/κ_{III} are the corresponding toughness values for pure mode II and III. The parameters, κ_{II} and κ_{III} , adjust the mode dependence. Criterion (7) can also be expressed as (5) with

$$\Gamma_C(\psi, \varphi) = \Gamma_{IC} [1 + (\kappa_{II} - 1) \sin^2 \psi \sin^2 \varphi + (\kappa_{III} - 1) \cos^2 \varphi]^{-1}. \quad (8)$$

The cut test: The delamination shape of the polyimide/glass interface induced by the cut in Fig. 2 was closely reproduced with $\kappa_{III} = 0.3$ (Jensen et al., 1990) corresponding to a mode III toughness about three times the mode I toughness for this interface.

Delamination orientation of bi-axially stressed thin films: With reference to Fig. 3, consider a thin isotropic elastic film bonded to a thick isotropic elastic substrate and subject to uniform in-plane stresses, σ_1 and σ_2 . Consider a straight delamination crack advancing in the film/substrate interface with orientation θ . For most orientations, the energy release rate has all three-mode components given by

$$G_I + G_{II} = \frac{(1 - \nu^2)h}{8E} [(\sigma_1 + \sigma_2)^2 + 2 \cos 2\theta (\sigma_1^2 - \sigma_2^2) + \cos^2 2\theta (\sigma_1 - \sigma_2)^2],$$

$$G_{III} = \frac{(1 + \nu)h}{4E} \sin^2 2\theta (\sigma_1 - \sigma_2)^2, \quad (9)$$

where E and ν are Young's modulus and Poisson's ratio of the film and h is its thickness. If the stress component in the bonded film perpendicular to the crack front is tensile, i.e., $\sigma_1 + \sigma_2 > (\sigma_1 - \sigma_2) \cos 2\theta$, the mode I stress intensity factor is positive, the crack-tip is open, and $\psi = \tan^{-1}(K_{II}/K_I)$ is given by plane strain solutions (Hutchinson and Suo, 1992). If this stress component is compressive, the crack-tip is closed ($K_I = 0$) and (9) is only valid if there is no frictional interaction between the crack faces. A normalized energy release

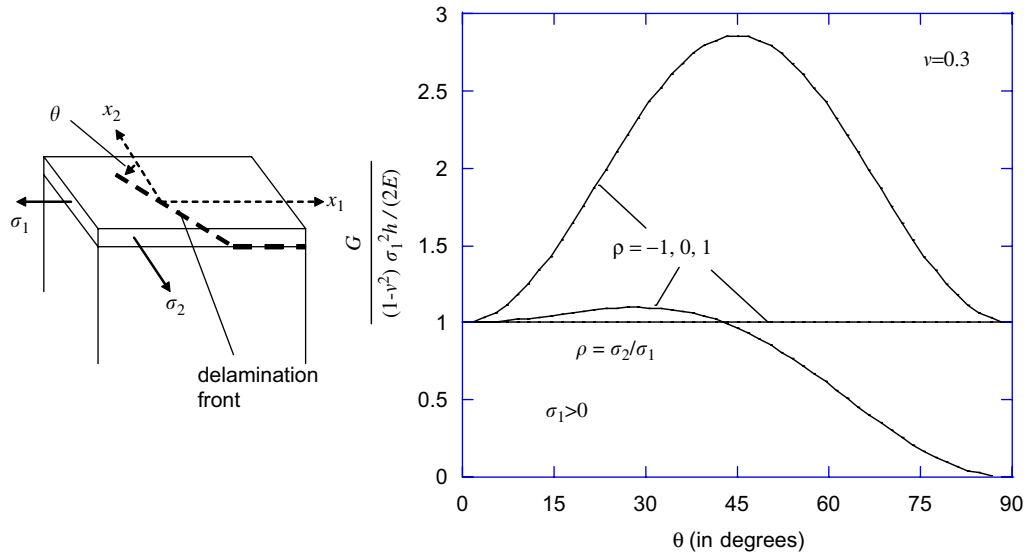


Fig. 3. Orientation dependence of the energy release rate of the delamination crack front for three in-plane biaxial stress states.

can be written as

$$\frac{G}{[(1-v^2)\sigma_1^2 h/(2E)]} = \frac{1}{4} \left[(1+\rho)^2 + 2\cos 2\theta(1-\rho^2) + \left(\cos^2 2\theta + \frac{2}{1-v} \sin^2 2\theta \right) (1-\rho)^2 \right] \quad (10)$$

with $\rho = \sigma_2/\sigma_1$.

For $\sigma_1 > 0$, the normalized energy release rate is plotted as a function of the delamination orientation in Fig. 3 for three stress states: uniaxial tension, $\rho = 0$; equi-biaxial tension, $\rho = 1$; and tension/compression with $\rho = -1$. All of these stress states can be achieved by combinations of residual or thermal stresses and superimposed stresses induced by overall deformation of the film/substrate system, as illustrated by a series of experiments conducted by Parry et al. (2004). There is no orientation dependence of G for equi-biaxial stressing (the curve for $\rho = 1$ is the horizontal line through 1 on the vertical scale). The surprising feature in Fig. 3 is the existence of the large maximum energy release rate for the tension/compression state ($\rho = -1$) at the orientation, $\theta = 45^\circ$, corresponding to a pure mode III delamination crack. For $|\theta| < 45^\circ$, $K_I > 0$ and the crack-tip is open, while for $45^\circ < \theta < 135^\circ$, the crack-tip is closed and $K_I = 0$.

The critical orientation of the delamination of a film in the tension/compression state ($\rho = -1$) provides an interesting illustration of the role of the mode III component in interface fracture. By definition, the critical orientation is the orientation in which the interface fracture criterion would first be attained if the stresses were increased monotonically and proportionally (with $\rho = -1$). If the interface toughness is mode-independent with $G = \Gamma_{IC}$ ($\kappa_{II} = \kappa_{III} = 1$), the critical orientation would be $\theta = 45^\circ$. At the other extreme, if the interface is assumed to be extremely tough in mode III with $\kappa_{III} \ll 1$, the critical orientation would be $\theta = 0^\circ$. To determine the critical orientation for arbitrary κ_{II} and κ_{III} , impose (5) with $\Gamma_C(\psi, \varphi)$ given by (8). From (6) and (9), $\tan \varphi = \sqrt{(1-v)/2} \cot 2\theta$. It can then be shown that the critical orientation, θ_C , is either 0° or 45° according to

$$\begin{aligned} \kappa_{III} &> \frac{1-v}{2} [1 - (1-\kappa_{II})\sin^2 \psi], & \theta_C &= 45^\circ, \\ \kappa_{III} &< \frac{1-v}{2} [1 - (1-\kappa_{II})\sin^2 \psi], & \theta_C &= 0^\circ \end{aligned} \quad (11)$$

as mapped in Fig. 4 for the case of no elastic mismatch between film and substrate which has $\psi = 52.1^\circ$ (Hutchinson and Suo, 1992). It should be possible to make use of the strong orientation dependence of the delamination of films in the tension/compression state to infer information on κ_{III} by observation of behavior for specific interfaces.

Critical conditions for propagation of corner interface flaws of thin films

Begley and Ambrico (2001) determined the energy release rate and the mode mix along the edge of a circular interface crack at the corner of the film/substrate system shown in Fig. 5. They restricted attention to systems whose second Dundurs' parameter can be neglected ($\beta = 0$). The film is stressed by thermal expansion mismatch with the substrate such that well away from the edge the state of stress in the interior of the film is equi-biaxial tension, σ . The energy release rate, G , at the centerline of the semi-circular crack and at one film thickness, h , from the free surface is plotted in Fig. 5 as a function of the normalized crack radius, a/h , for several values of the first Dundurs' parameter. The distribution of the mode mix around the crack edge is also plotted for two values of a/h (K_I is positive around the entire circumference of the crack if $\sigma > 0$). Two features stand out. The energy release rate is greatest in the vicinity where the crack intersects the free surface, and the mode III component contributes significantly to the energy release rate near this location. Begley and Ambrico (2001) also determined G and mode mix at the corner crack of a film that is bonded to the interior of the substrate surface (i.e., the film edge is not flush with the substrate edge) and for a half-penny shaped interface crack at the edge of a film bonded to a substrate. The qualitative features noted for the flush corner flaw in Fig. 5 pertain to these other cases as well.

If the crack propagation condition is based on a critical energy release rate, $G = \Gamma_{IC}$, independent of the mode combination, the critical condition for interface crack propagation would first be attained where the corner flaw meets the free surface. However, if the interface is relatively tough in mode III (i.e., $\kappa_{III} \ll 1$), then the critical location for the onset of propagation will be some interior location along the crack edge.

Mode III effects in the presence of plastic yielding: When delamination occurs along an interface between an elastic-plastic material and an elastic substrate, the plastic yielding of the adjacent material is expected to have a strong effect on crack growth. For homogeneous elastic-plastic materials studies of mode I, II and III crack-tip fields for stationary cracks have been carried out by Pan and Shih (1992), and ductile crack growth in mixed-mode I/III has been analyzed by Gao and Shih (1998), where the underlying mechanism is void growth. In the present paper for mixed-mode crack growth along an interface between dissimilar materials, the fracture mechanism at the interface is represented by a cohesive zone model.

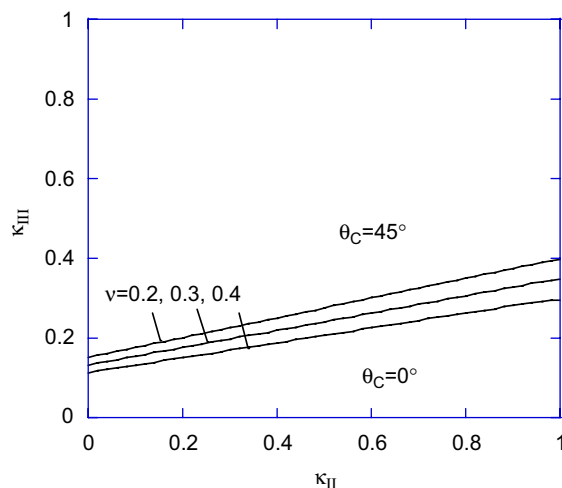


Fig. 4. Critical orientation of the delamination crack front as determined by the two parameters, κ_I and κ_{II} , of the mixed mode interface fracture criterion. Above the line, the critical orientation is 45° to the maximum tensile stress direction, x_1 ; below the line the front is perpendicular to the x_1 -direction. Plotted for the case of no elastic mismatch between the film and substrate.

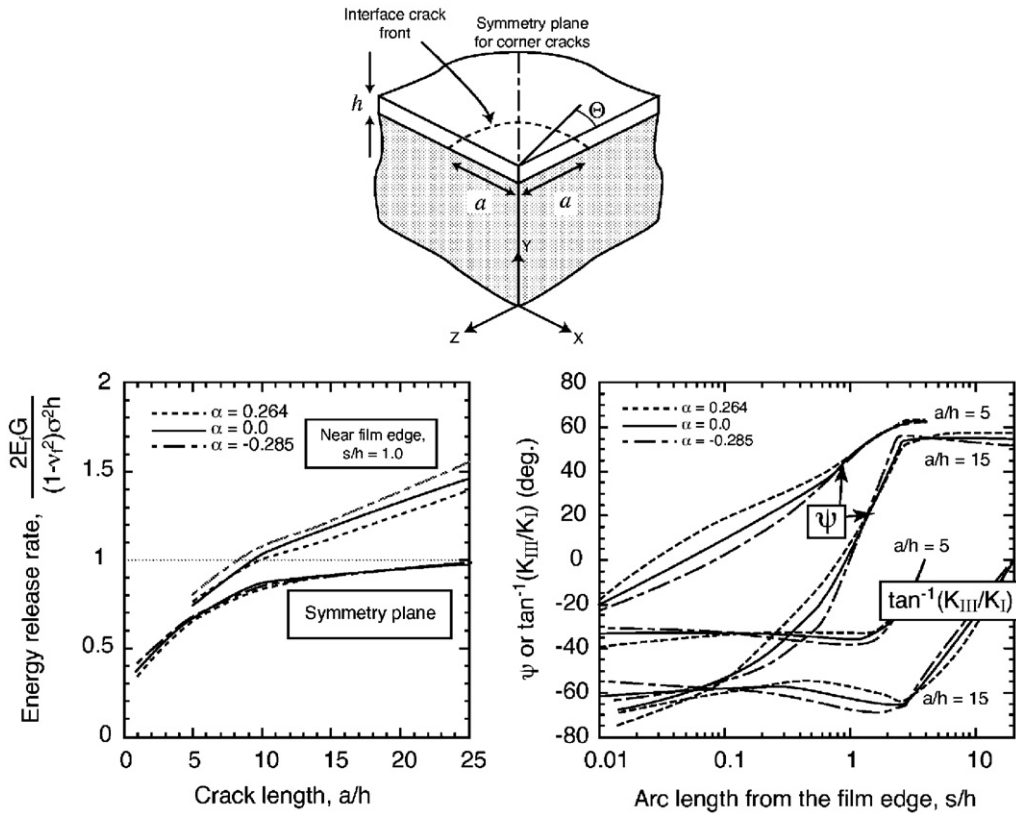


Fig. 5. Results of Begley and Ambrico (2001) for the energy release rate at two locations and the distribution of mode mix for a corner penny-shaped crack at the interface between a film and substrate for three values of the Dundurs' mismatch parameter, α . The film is under equi-biaxial tension σ well away from the edges. The phase angle measure for mode III in this figure is $\tan^{-1}(K_{III}/K_I)$. (Begley and Ambrico employ a different definition of φ than the present one.) Mode III is the dominant intensity contribution over the crack front near the edge.

2. Problem formulation and analysis

The interface crack growth analyses under mixed modes I, II and III loading are carried out for conditions of small-scale yielding. The substrate (see Fig. 6) is taken to be elastic with Young's modulus E_2 and Poisson's ratio ν_2 , while material no. 1 above the interface is elastic-plastic, with the elastic properties E_1 and ν_1 , the uniaxial yield stress σ_{Y1} and the strain hardening exponent N_1 . This material is described by a finite strain generalization of J_2 -flow theory (Hutchinson, 1973), with the uniaxial true stress-natural strain curve represented by a piecewise power law

$$\varepsilon = \begin{cases} \frac{\sigma}{E} & \sigma \leq \sigma_{Y1}, \\ \frac{\sigma_{Y1}}{E} \left(\frac{\sigma}{\sigma_{Y1}} \right)^{1/N_1} & \sigma > \sigma_{Y1}. \end{cases} \quad (12)$$

The plane strain elastic mixed modes I and II interface crack problem was solved long ago by many authors (e.g. England, 1965). The plane strain solution remains relevant here, since the transverse strain in the x_3 -direction is taken to be zero. Following the formulation of Rice (1988) (see also Tvergaard and Hutchinson, 1993), the crack has tractions acting on the interface in the x_1 - x_2 -plane, which are given in terms of the two stress intensity factor components, K_I and K_{II} , by

$$\sigma_{22} + i\sigma_{12} = (K_I + iK_{II})(2\pi r)^{-1/2} r^{ie}. \quad (13)$$

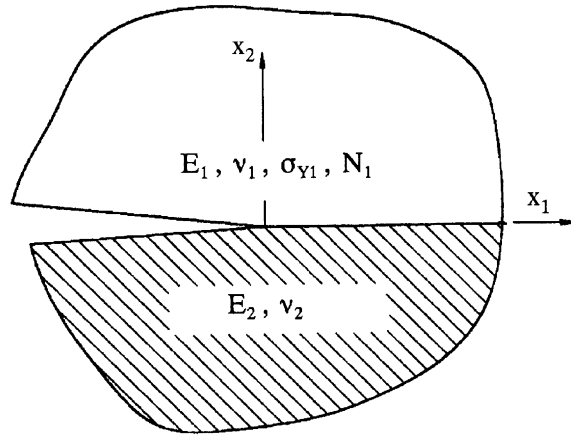


Fig. 6. Interface crack with elastic-plastic material properties above the interface and elastic properties below.

Here, r is the distance from the tip, $i = \sqrt{-1}$, ε is the oscillation index

$$\varepsilon = \frac{1}{2\pi} \ln \left(\frac{1 - \beta}{1 + \beta} \right) \tag{14}$$

and β is the second Dundurs' parameter

$$\beta = \frac{1}{2} \frac{\mu_1(1 - 2\nu_2) - \mu_2(1 - 2\nu_1)}{\mu_1(1 - \nu_2) + \mu_2(1 - \nu_1)}, \tag{15}$$

where the shear moduli are $\mu_1 = E_1/(2(1 + \nu_1))$ and $\mu_2 = E_2/(2(1 + \nu_2))$.

The elastic stresses corresponding to the mode III problem are uncoupled to the in-plane components (13), and the corresponding tractions on the interface are

$$\sigma_{23} = K_{III}(2\pi r)^{-1/2}. \tag{16}$$

The relation between the energy release rate and the magnitudes of the stress intensity factors is given by (2). It will subsequently be convenient to let

$$|K| = \sqrt{K_I^2 + K_{II}^2}. \tag{17}$$

With a reference length L chosen to characterize the remote field, an L -dependent measure of I–II mode mixity ψ is defined by

$$\tan \psi = \frac{\text{Im}[(K_I + iK_{II})L^{i\varepsilon}]}{\text{Re}[(K_I + iK_{II})L^{i\varepsilon}]}, \tag{18}$$

which reduces to the more familiar measure, $\tan \psi = K_{II}/K_I$, when $\varepsilon = 0$. The displacement components associated with the I–II singularity field, with amplitude $|K|$, are specified in Tvergaard and Hutchinson (1993), and the displacement fields corresponding to mode III are

$$u_3 = \frac{2K_{III}}{\mu_i} (r/2\pi)^{1/2} \sin(\theta/2), \tag{19}$$

where μ_i equals μ_1 or μ_2 , above or below the interface. It is noted that inside a short cohesive zone the oscillation form of (13) has little effect, but this oscillation form still exists in the outer fields.

The x_1 -axis is in the crack plane and the initial crack-tip is located at $x_1 = x_2 = 0$ (see Fig. 6). The traction–separation relation used to model the fracture process (Fig. 7) is specified everywhere on the boundary $x_1 > 0, x_2 = 0$ of the region analyzed, while zero tractions are specified for $x_1 \leq 0, x_2 = 0$.

The traction–separation law used by Tvergaard and Hutchinson (1993) is a special version of that proposed by Tvergaard (1990) as a generalization of the model of Needleman (1987). Here, the model is further

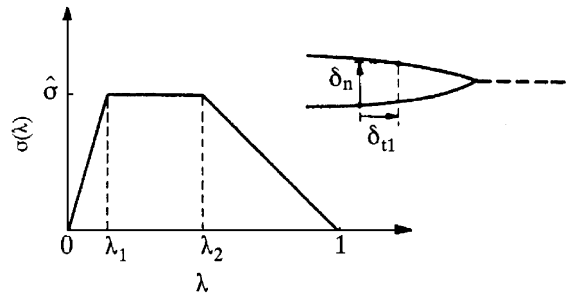


Fig. 7. Specification of traction–separation relation.

extended to account for tangential separation in two perpendicular directions, so that δ_n , δ_{t1} and δ_{t3} denote the normal and tangential components of the relative displacement of the crack faces across the interface in the zone where the fracture processes are occurring (Fig. 7). Here, δ_{t3} denotes the tangential separation in the direction parallel to the crack front. When δ_n^c , δ_{t1}^c and δ_{t3}^c are critical values of these displacement components and a single nondimensional separation measure is defined as $\lambda = [(\delta_n/\delta_n^c)^2 + (\delta_{t1}/\delta_{t1}^c)^2 + (\delta_{t3}/\delta_{t3}^c)^2]^{1/2}$ the tractions drop to zero when $\lambda = 1$. With $\sigma(\lambda)$ displayed in Fig. 7, a potential from which the tractions are derived is defined as

$$\Phi(\delta_n, \delta_{t1}, \delta_{t3}) = \delta_n^c \int_0^\lambda \sigma(\lambda') d\lambda'. \quad (20)$$

The normal component and the two tangential components of the traction acting on the interface in the fracture process zone are given by

$$T_n = \frac{\partial \Phi}{\partial \delta_n} = \frac{\sigma(\lambda) \delta_n}{\lambda \delta_n^c}, \quad T_{t1} = \frac{\partial \Phi}{\partial \delta_{t1}} = \frac{\sigma(\lambda) \delta_{t1} \delta_n^c}{\lambda \delta_{t1}^c \delta_n^c}, \quad T_{t3} = \frac{\partial \Phi}{\partial \delta_{t3}} = \frac{\sigma(\lambda) \delta_{t3} \delta_n^c}{\lambda \delta_{t3}^c \delta_n^c}. \quad (21)$$

The peak normal traction under pure normal separation is $\hat{\sigma}$, and the peak shear tractions are $(\delta_n^c/\delta_{t1}^c)\hat{\sigma}$ or $(\delta_n^c/\delta_{t3}^c)\hat{\sigma}$ in pure tangential separation in the x_1 or the x_3 -directions, respectively. The work of separation per unit area of interface is given by Eq. (20) with $\lambda = 1$, and for the separation function $\sigma(\lambda)$ in Fig. 7 the work is

$$\Gamma_0 = \frac{1}{2} \hat{\sigma} \delta_n^c (1 - \lambda_1 + \lambda_2). \quad (22)$$

It has been found in Tvergaard and Hutchinson (1992, 1993) that the two most important parameters characterizing the fracture process in this model are Γ_0 and $\hat{\sigma}$. Scheider and Brocks (2003) have found cases where also differences in the shape of the separation law have an important effect.

Here the interest is in metal–ceramic interfaces, but the parameter values to be used in the cohesive zone model (20)–(22) are not based on direct measurements. For glass–epoxy interfaces there has been more detailed experimental studies (Liechti et al., 1992). In a recent study of a sapphire–epoxy interface with the sapphire enhanced by coating (Mello and Liechti, 2006) it has been found that the toughness Γ_0 varies with the mode mix, in contrast to the assumption in (20)–(22). Such mode dependent toughness has also been found for adhesives (Högberg, 2006), and it is noted that this possibility is incorporated in the model of Tvergaard (1990).

For $K_{III} = 0$, a reference stress intensity factor is defined as

$$K_0 = \left[\frac{1 - \nu_1^2}{E_1} + \frac{1 - \nu_2^2}{E_2} \right]^{-1/2} \left(\frac{2\Gamma_0}{1 - \beta^2} \right)^{1/2}, \quad (23)$$

which is the value of $|K|$ needed to advance the interface crack in the absence of any plasticity. This value is independent of ψ since a potential is used to generate the relation of tractions to crack face displacements of the interface. A length quantity R_0 , which scales with the size of the plastic zone in material no. 1 (when

$|K| \cong K_0$ and $K_{III} = 0$), is defined by

$$R_0 = \frac{1}{3\pi} \left(\frac{K_0}{\sigma_{Y1}} \right)^2 = \frac{2}{3\pi} \left[\frac{1 - \nu_1^2}{E_1} + \frac{1 - \nu_2^2}{E_2} \right]^{-1} \frac{\Gamma_0}{(1 - \beta^2)\sigma_{Y1}^2}, \tag{24}$$

while the mode I–II mixity measure ψ refers to the distance L from the tip, it is natural to define a reference measure of mixity, ψ_0 , based on the reference length R_0 . The relation between ψ_0 and ψ is

$$\psi_0 = \psi + \varepsilon \ln(R_0/L). \tag{25}$$

3. Numerical method

Finite strains are accounted for in the numerical analyses, using a Lagrangian convected coordinate formulation of the field equations. In this formulation, a material point is identified in the reference configuration by x_i . The contravariant components of the Cauchy stress tensor σ^{ij} and the Kirchhoff stress tensor τ^{ij} are related by $\tau^{ij} = \sqrt{G/g}\sigma^{ij}$. The metric tensors in the current and the reference configuration are denoted by G_{ij} and g_{ij} , with the determinants G and g , respectively, and the incremental stress–strain relationship is of the form $\dot{\tau}^{ij} = L^{ijkl}\dot{\eta}_{kl}$, where L^{ijkl} are the instantaneous moduli.

The Lagrangian strain tensor is given in terms of the displacement components u^i on the reference base vectors by

$$\eta_{ij} = \frac{1}{2}(u_{i,j} + u_{j,i} + u_{,i}^k u_{k,j}), \tag{26}$$

where $(\)_j$ denotes covariant differentiation in the reference frame. Numerical solutions are obtained by a linear incremental solution procedure, by expanding the principle of virtual work about the current state. The incremental equation is, to lowest order, equal to

$$\int_V \{ \Delta\tau^{ij} \delta\eta_{ij} + \tau^{ij} \Delta u_{,i}^k \delta u_{k,j} \} dV = \int_A \Delta T^i \delta u_i dA - \left[\int_V \tau^{ij} \delta\eta_{ij} dV - \int_A T^i \delta u_i dA \right]. \tag{27}$$

Here, V and A are, respectively, the volume and surface of the body in the reference configuration, $\Delta\tau^{ij}$ and $\Delta\eta_{ij}$ are the stress and strain increments, T^i are contravariant components of the nominal surface tractions, etc. The bracketed terms are equilibrium corrections. More details of the crack growth procedure can be found in Tvergaard and Hutchinson (1993) and Tvergaard (2001).

The displacement fields are approximated in terms of special planar 8-noded isoparametric elements, with three degrees of freedom in each nodal point, but with the transverse strain in the x_3 -direction taken to be zero. The volume integral in Eq. (27) is carried out by using 2×2 integration points within each element.

A circular region with radius A_0 is analyzed numerically. Fig. 8 illustrates the initial near-tip mesh in the center of the region analyzed, with 80×4 uniform quadrilaterals along the interface in the range where crack growth is studied. The length of one square element inside the uniform mesh is denoted Δ_0 , and the initial

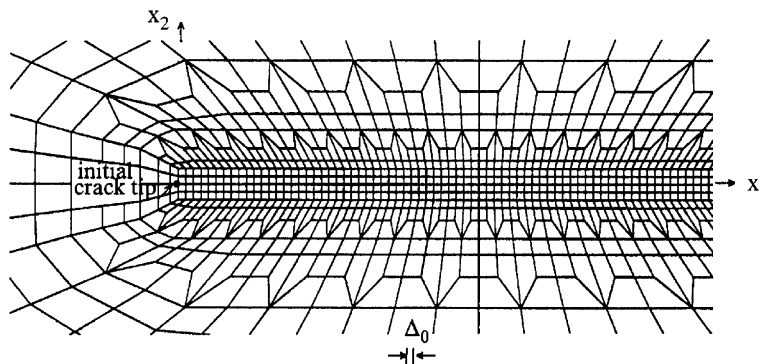


Fig. 8. Mesh used for some of the crack growth analyses.

crack-tip is located at $x_1 = 0$. The outer radius is chosen to be $A_0 = 800\,000\Delta_0$, in order that the plastic zone size should be well below $A_0/10$.

4. Results

The crack growth analyses carried out here consider an elastic-plastic material no. 1 characterized by the parameters $\sigma_{Y1}/E_1 = 0.003$, $\nu_1 = \frac{1}{3}$ and $N_1 = 0.1$, while the elastic substrate has $E_2/E_1 = 2$ and $\nu_2 = \frac{1}{3}$ in the first analyses. In the traction–separation law the values $\delta_n^c/\delta_{t1}^c = 1$, $\delta_n^c/\delta_{t2}^c = 1$, $\delta_n^c = 0.1\Delta_0$, $\lambda_1 = 0.15$ and $\lambda_2 = 0.50$ are used, while $\hat{\sigma}/\sigma_{Y1}$ is varied. Also, in all the cases analyzed, the load is applied in such a manner that stress intensity ratio $K_{III}/|K|$ remains constant. The load is applied on the outer boundary in the form of displacements according to the elastic singularity field.

Fig. 9 shows examples of crack growth resistance curves for $\hat{\sigma}/\sigma_{Y1} = 3.0$, $\psi_0 = -2.2^\circ$ and different values of $K_{III}/|K|$. In relation to the near-tip mesh in Fig. 8 it is noted that here $R_0/\Delta_0 = 10.82$. The curves show the energy release rate G according to (2) vs. the amount of crack growth Δa , normalized by Γ_0 and R_0 , respectively. It is seen that here the lowest fracture toughness occurs for $K_{III} = 0$, and the fracture toughness increases as the value of $K_{III}/|K|$ is increased. For all three curves, very shallow maxima occur in the vicinity of $\Delta a/R_0 \approx 0.4$.

Variations of the steady-state toughness G_{ss}/Γ_0 vs. $K_{III}/|K|$ are shown in Fig. 10 for the material parameters also considered in Fig. 9. The values of G_{ss}/Γ_0 are calculated as the maxima of the corresponding crack growth resistance curves, and thus the curve for $\psi_0 = -2.2^\circ$ in Fig. 10 contains the maxima of the curves in Fig. 9. For $\psi_0 = 15.0^\circ$ the fracture toughness increases more rapidly as a function of $K_{III}/|K|$, but for $\psi_0 = -10.8^\circ$ the fracture toughness increases less rapidly. For $\psi_0 = -19.4^\circ$ the value of G_{ss}/Γ_0 first decays slightly, and then starts to increase strongly, as the value of $K_{III}/|K|$ increases from zero, and the same type of behavior is even more pronounced for $\psi_0 = -28.0^\circ$. Results are only shown for positive values of $K_{III}/|K|$, as the curves are symmetric with respect to the vertical axis in Fig. 10.

The five points shown in Fig. 10 as intersections of the curves with the vertical axis, i.e., values for $K_{III}/|K| = 0$, are the plane strain results, as has been investigated previously (Tvergaard and Hutchinson, 1993; Tvergaard, 2001). In agreement with the earlier results it is seen that the smallest value occurs for $\psi_0 = -2.2^\circ$, where the conditions at the crack-tip are near mode I, and that the fracture toughness grows when the contribution of K_{II} is increased, both in the positive and negative directions.

The behavior found for $\psi_0 = -19.4^\circ$ in Fig. 10 is further investigated in Fig. 11 by varying the value of δ_n^c/δ_{t1}^c , while $\delta_{t2}^c = \delta_{t1}^c$. Thus, for $\delta_n^c/\delta_{t1}^c = 2$ the peak stress in pure tangential separation is two times that in pure normal separation, according to (21), and it is seen in Fig. 11 that this gives a somewhat higher fracture toughness. For $\delta_n^c/\delta_{t1}^c = \frac{1}{2}$ the peak stress in pure tangential separation is half that in pure normal separation,

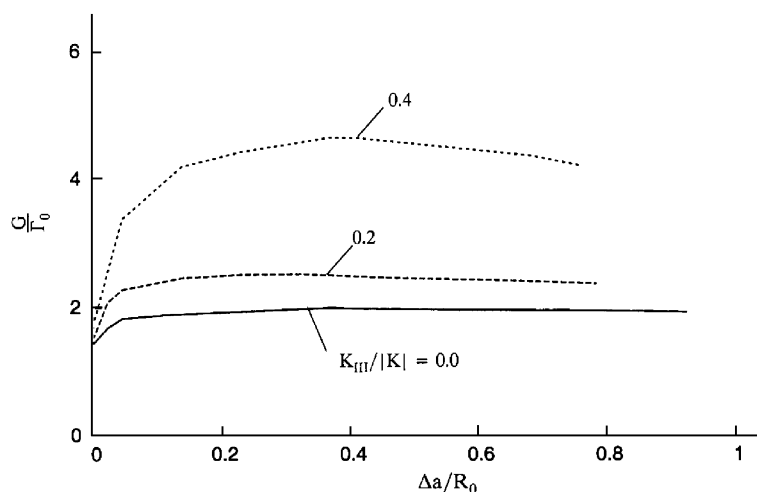


Fig. 9. Interface crack growth resistance curves for $\hat{\sigma}/\sigma_{Y1} = 3.0$, $E_2/E_1 = 2$, $\psi_0 = -2.2^\circ$ and different values of $K_{III}/|K|$.

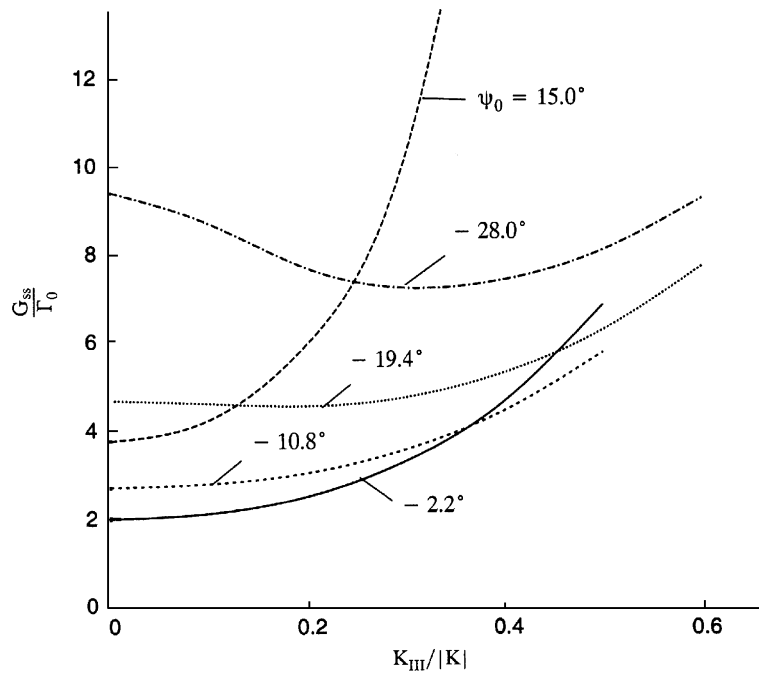


Fig. 10. Steady-state interface toughness as a function of $K_{III}/|K|$, for five different values of the local mixity measure ψ_0 . The elastic modulus mismatch is specified by $E_2/E_1 = 2$ and the interface strength is $\hat{\sigma}/\sigma_{Y1} = 3.0$.

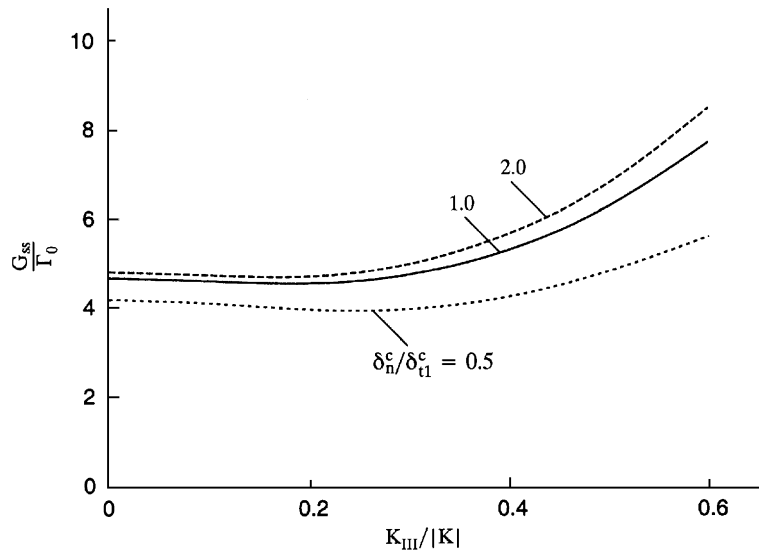


Fig. 11. Steady-state interface toughness as a function of $K_{III}/|K|$, for $\psi_0 = -19.4^\circ$ and for three different values of δ_n^c/δ_{t1}^c . For $\delta_n^c/\delta_{t1}^c = 2$ the peak stress in pure tangential separation is two times that in pure normal separation, while for $\delta_n^c/\delta_{t1}^c = \frac{1}{2}$ the tangential peak stress is half that in normal separation. Other interface parameters are $E_2/E_1 = 2$ and $\hat{\sigma}/\sigma_{Y1} = 3.0$.

leading to a lower fracture toughness. But in both cases the curves follow the general shape of that for $\delta_n^c/\delta_{t1}^c = 1$, and thus the occurrence of the minimum fracture toughness for a nonzero value of $K_{III}/|K|$ does not depend on choosing the same traction–separation relation in pure tangential separation as that in pure normal separation. It is noted that a variation of δ_n^c/δ_{t1}^c was also considered in Tvergaard and Hutchinson (1993) for the

plane strain problem, where it was also found that the fracture toughness was more reduced by taking $\delta_n^c/\delta_{t1}^c = \frac{1}{2}$ than increased by taking a ratio much higher than 2.

In Fig. 12, a higher mismatch of the elastic moduli is considered, $E_2/E_1 = 6$, but otherwise all material parameters and interface parameters are the same as those considered in Fig. 10. It is seen that the higher mismatch gives generally higher fracture toughnesses, as was also found for the plane strain problem (Tvergaard, 2001). Qualitatively, the trends agree with those found in Fig. 10, in that the fracture toughness increases rapidly with increasing value of $K_{III}/|K|$ for $\psi_0 = 15.2^\circ$. For smaller values of ψ_0 this increase becomes weaker, and for $\psi_0 = -19.1^\circ$ the toughness reaches a minimum at $K_{III}/|K| \approx 0.3$ before the increase starts. Again, for the plane strain problem, $K_{III}/|K| = 0$, the smallest fracture toughness is reached at $\psi_0 = 0.3^\circ$, near pure mode I conditions at the crack-tip, while an increased influence of K_{II} gives higher toughness.

Fig. 13 has all material parameters identical to those in Fig. 12, except that the peak stress in the traction separation law for the interface is reduced, $\hat{\sigma}/\sigma_{Y1} = 2.5$. This reduces the general level of the fracture toughnesses below those in Fig. 12, and also below those in Fig. 10. The dependence on different values of ψ_0 agrees with the results in the previous figures. For the smallest value, $\psi_0 = -22.6^\circ$, the curve has become very flat, indicating that a minimum of G would be found at a nonzero value of K_{III} if a larger negative value of ψ_0 was considered.

We further investigate the local minimum of G_{ss}/Γ_0 at a finite value of $K_{III}/|K|$ found in Figs. 10–13 that for larger negative values of ψ_0 . Results for a homogeneous solid are illustrated in Fig. 14. Thus, material nos. 1 and 2 are identical, elastic-plastic, with $E_2/E_1 = 1$, $\sigma_{Y2}/\sigma_{Y1} = 1$, etc. and with $\sigma_{Y1}/E_1 = 0.003$, $\nu_1 = \frac{1}{3}$ and $N_1 = 0.1$. Only crack growth on the initial crack plane is permitted. The curves in Fig. 14 are obtained for $\psi_0 = -22.92^\circ$, where the previous figures show a local minimum at a finite value of $K_{III}/|K|$. However, in Fig. 14 the fracture toughness increases monotonically as a function of $K_{III}/|K|$. Also, in the homogeneous solid the behavior found for a negative value of ψ_0 , as in Fig. 14, is necessarily identical to the behavior found for the same positive value of ψ_0 . This indicates that the strong differences between positive and negative values of ψ_0 in Figs. 10–13 are a result of the asymmetry associated with the material mismatch along the interface, which gives strong differences in the elastic-plastic near-tip fields in material no. 1, while the substrate remains elastic.

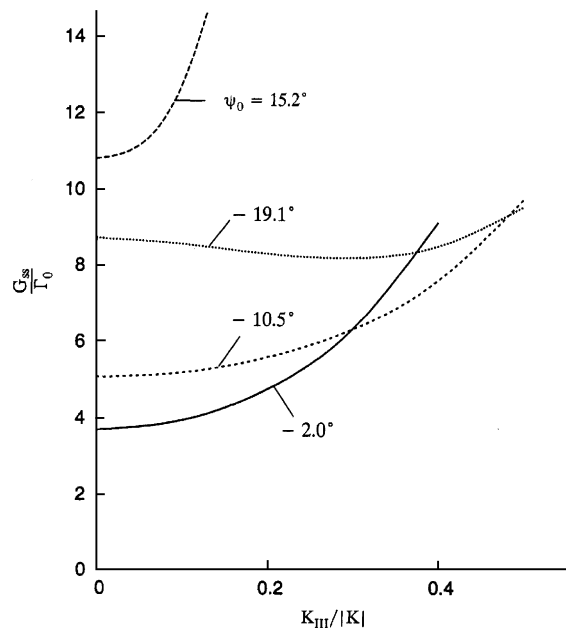


Fig. 12. Steady-state interface toughness as a function of $K_{III}/|K|$, for four different values of the local mixity measure ψ_0 . The elastic modulus mismatch is specified by $E_2/E_1 = 6$ and the interface strength is $\hat{\sigma}/\sigma_{Y1} = 3.0$.

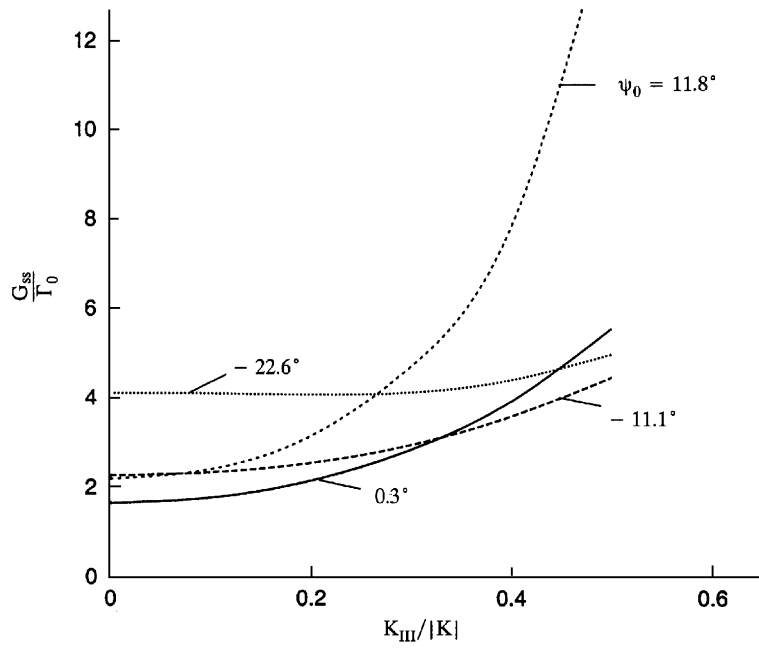


Fig. 13. Steady-state interface toughness as a function of $K_{III}/|K|$, for four different values of the local mixity measure ψ_0 . The elastic modulus mismatch is specified by $E_2/E_1 = 6$ and the interface strength is $\hat{\sigma}/\sigma_{Y1} = 2.5$.

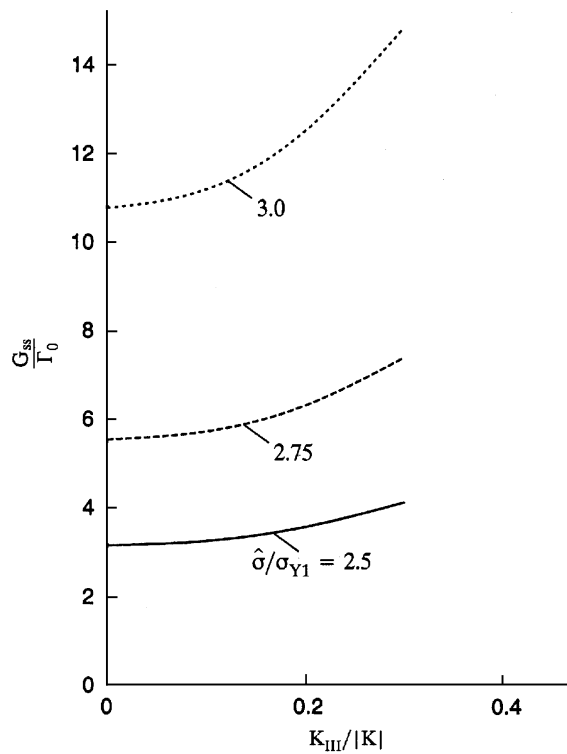


Fig. 14. Results for a homogeneous solid, $E_2/E_1 = 1$ and $\sigma_{Y2}/\sigma_{Y1} = 1$. Steady-state toughness as a function of $K_{III}/|K|$, for three different values of $\hat{\sigma}/\sigma_{Y1}$, when $\psi_0 = -22.92^\circ$.

5. Summary

In this paper, trends in toughness of interfaces as dependent on the mode III stress intensity factor have been explored using a model that employs mixed mode cohesive separation along the interface. The focus is on interfaces joining elastic and elastic-plastic solids subject to mixed mode loadings with all three components of stress intensity present. Interface loadings are considered with all three components increased proportionally. Examples discussed in the Introduction illustrate that mode III makes a significant contribution to the energy release in a number of thin film delamination problems, particularly at cuts, edges and corners. The dependence of the interface toughness on the mode III component determines whether or not these locations are the critical for initiating delamination: a strong positive dependence on mode III deters local criticality, while a weak or negative dependence leads to local susceptibility.

If the materials on either side of the interface are identical elastic-plastic solids, the model predicts that the presence of a mode III component gives rise to a tougher interface for all mixed mode combinations investigated. The presence of mode III also increases interface toughness for combined loading of the interface in which one material is elastic and the other is elastic-plastic when the mode II component is nonnegative ($\psi_0 \geq 0$, with the elastic-plastic material above the interface as in Fig. 6). However, the toughness of such interfaces is lowered due to mode III for negative mode II components ($\psi_0 < 0$). Thus, there are cases in which the presence of a mode III component will weaken the interface, making it more susceptible to delamination in locations where mode III is present. The asymmetry with respect to the sign of mode II is a consequence of the asymmetry of the materials across the interface since the behavior is independent of the sign of the mode II component when identical materials lie above and below the interface. It is noted that cases where the fracture toughness is reduced in the presence of a mode III component have also been found by Gao and Shih (1998), based on a void growth fracture mechanism.

References

- Banks-Sills, L., Travitzky, N., Ashkenazi, R., Eliasi, R., 1999. A methodology for measuring interface fracture toughness of composite materials. *Int. J. Fract.* 99, 143–161.
- Begley, M.R., Ambrico, J.M., 2001. Delamination of thin films from two-dimensional interface flaws at corners and edges. *Int. J. Fract.* 112, 205–222.
- Chai, H., 1990. Three-dimensional fracture analysis of thin-film debonding. *Int. J. Fract.* 46, 237–256.
- England, A.H., 1965. A crack between dissimilar media. *J. Appl. Mech.* 32, 400–402.
- Evans, A.G., Hutchinson, J.W., 1989. Effect of non-planarity on the mixed mode fracture resistance of bimaterial interfaces. *Acta Metall.* 37, 909–916.
- Gao, X., Shih, C.F., 1998. A parametric study of mixed-mode I/III ductile fracture in tough materials under small scale yielding. *Eng. Fract. Mech.* 60, 407–420.
- Högberg, J.L., 2006. Mixed mode cohesive law. *Int. J. Fract.* 141, 549–559.
- Hutchinson, J.W., 1973. Finite strain analysis of elastic-plastic solids and structures. In: Hartung, R.F. (Ed.), *Numerical Solution of Nonlinear Structural Problems*. ASME, New York, p. 17.
- Hutchinson, J.W., Suo, Z., 1992. Mixed mode cracking in layered materials. *Adv. Appl. Mech.* 29, 63–191.
- Jensen, H.M., Hutchinson, J.W., Kim, K.-S., 1990. Decohesion of a cut prestressed film on a substrate. *Int. J. Solids Struct.* 26, 1099–1114.
- Liechti, K.M., Chai, Y.S., 1992. Asymmetric shielding in interfacial fracture under in-plane shear. *J. Appl. Mech.* 59, 295.
- Liechti, K.M., Chai, Y.S., Liang, Y.-M., 1992. Three-dimensional effects in interfacial crack propagation. *Exp. Mech.* 32, 218–224.
- Mello, A.W., Liechti, K.M., 2006. The effect of self-assembled monolayers on interfacial fracture. *J. Appl. Mech.* 73, 860–870.
- Needleman, A., 1987. A continuum model for void nucleation by inclusion debonding. *J. Appl. Mech.* 54, 525–531.
- Pan, J., Shih, C.F., 1992. Elastic-plastic analysis of combined mode I, II and III crack-tip fields under small-scale yielding conditions. *Int. J. Solids Struct.* 29, 2795–2814.
- Parry, G., Coupeau, C., Colin, J., Cimetiere, A., Grilhe, J., 2004. Buckling and post-buckling of stressed straight-sided wrinkles: experimental AFM observations of bubbles formation and finite element simulations. *Acta Mater.* 52, 3959–3966.
- Rice, J.R., 1988. Elastic fracture mechanics concepts for interfacial cracks. *J. Appl. Mech.* 55, 98–103.
- Scheider, I., Brocks, W., 2003. The effect of the traction separation law on the results for cohesive zone crack propagation analyses. *Key Eng. Mater.* 251–252, 313–318.
- Tvergaard, V., 1990. Effect of fibre debonding in a whisker-reinforced metal. *Mater. Sci. Eng. A* 125, 203–213.
- Tvergaard, V., 2001. Resistance curves for mixed mode interface crack growth between dissimilar elastic-plastic solids. *J. Mech. Phys. Solids* 49, 2689–2703.

- Tvergaard, V., Hutchinson, J.W., 1992. The relation between crack growth resistance and fracture process parameters in elastic-plastic solids. *J. Mech. Phys. Solids* 40, 1377–1397.
- Tvergaard, V., Hutchinson, J.W., 1993. The influence of plasticity on mixed mode interface toughness. *J. Mech. Phys. Solids* 41, 1119–1135.
- Yang, Q.D., Thouless, M.D., 2001. Mixed mode fracture analyses of plastically-deforming adhesive joints. *Int. J. Fract.* 110, 175–187.